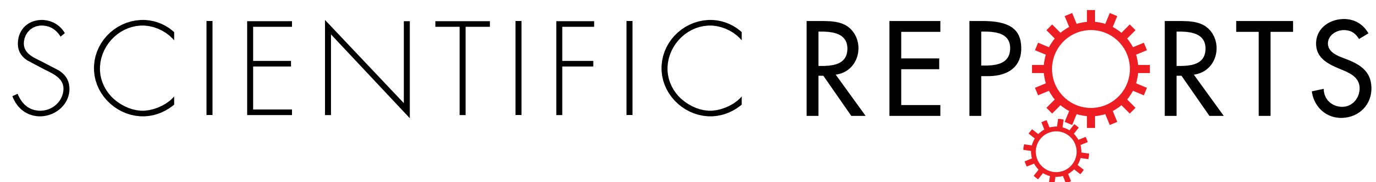

OPEN

Spin-dependent transport properties of $Fe_3O_4/MoS_2/Fe_3O_4$ junctions

Received: 08 June 2015
Accepted: 24 September 2015
Published: 02 November 2015

Han-Chun Wu[1], Cormac Ó Coileáin[1,2,3], Mourad Abid[2], Ozhet Mauit[3], Askar Syrlybekov[3,4], Abbas Khalid[3], Hongjun Xu[3], Riley Gatensby[5], Jing Jing Wang[3], Huajun Liu[6], Li Yang[7], Georg S. Duesberg[5], Hong-Zhou Zhang[3], Mohamed Abid[2] & Igor V. Shvets[3]

Magnetite is a half-metal with a high Curie temperature of 858 K, making it a promising candidate for magnetic tunnel junctions (MTJs). Yet, initial efforts to exploit its half metallic nature in Fe_3O_4/MgO/Fe_3O_4 MTJ structures have been far from promising. Finding suitable barrier layer materials, which keep the half metallic nature of Fe_3O_4 at the interface between Fe_3O_4 layers and barrier layer, is one of main challenges in this field. Two-dimensional (2D) materials may be good candidates for this purpose. Molybdenum disulfide (MoS_2) is a transition metal dichalcogenide (TMD) semiconductor with distinctive electronic, optical, and catalytic properties. Here, we show based on the first principle calculations that Fe_3O_4 keeps a nearly fully spin polarized electron band at the interface between MoS_2 and Fe_3O_4. We also present the first attempt to fabricate the $Fe_3O_4/MoS_2/Fe_3O_4$ MTJs. A clear tunneling magnetoresistance (TMR) signal was observed below 200 K. Thus, our experimental and theoretical studies indicate that MoS_2 can be a good barrier material for Fe_3O_4 based MTJs. Our calculations also indicate that junctions incorporating monolayer or bilayer MoS_2 are metallic.

Magnetite (Fe_3O_4), an archetypal oxide with potential applications in spintronics, has attracted a tremendous level of attention in recent decades. It has a nearly fully spin polarized electron band at the Fermi level (half-metallic character) and a high Curie temperature of 858 K, which make it a promising candidate for room temperature spintronic devices and applications[1–3]. Recently, interesting spin transport properties in Fe_3O_4 have been reported, i.e., a spin Seebeck effect[4], a spin filter effect[5], an electrical field-induced phase transition[6–8], large transversal magnetoresitance (MR)[9,10], and charge-orbital ordering driven magnetic state switching in Fe_3O_4/MgO/Fe_3O_4 junctions[11]. Yet, initial efforts to exploit its half metallic nature in magnetic tunnel junction (MTJ) structures have been far from promising[11–13]. The reduced MR attained in these investigations was attributed to the formation of a dead layer at the interface between Fe_3O_4 layers and MgO barrier layer, which reduces the spin polarization. Finding suitable barrier layer materials is one of main challenges in this field.

Two-dimensional (2D) materials may be good candidates for this purpose. For example, graphene, an atomic-thick carbon sheet[14–15], shows great potential for enhancing spin polarization. A recent experiment showed that spin dependent transport at the interfaces of Fe_3O_4-graphene-Fe_3O_4 junctions contributes −1.6% MR to the whole device[16]. This effect can be further enhanced by inserting a thin oxide layer such as TiO_2[17]. Unlike graphene, molybdenum disulfide (MoS_2) is a transition metal dichalcogenide semiconductor. Monolayer MoS_2 is a direct band gap semiconductor with a band gap of 1.9 eV[18], while

[1]Key Laboratory of Cluster Science of Ministry of Education, School of Physics, Beijing Institute of Technology, Beijing, 100081, P.R. China. [2]KSU-Aramco Center, King Saud University, Riyadh 11451, Saudi Arabia. [3]School of Physics and CRANN, Trinity College Dublin, Dublin 2, Ireland. [4]National Laboratory Astana, Nazarbayev University, Astana, Kazakhstan. [5]CRANN, School of Chemistry, Trinity College Dublin, Dublin 2, Ireland. [6]Institute of Plasma Physics, Chinese Academy of Sciences, Hefei, 230031, P. R. China. [7]Electronic Engineering Institute, Hefei, 230037, P. R. China. Correspondence and requests for materials should be addressed to H.-C.W. (email: wuhc@bit.edu.cn) or H.J.L. (email: liuhj@ipp.ac.cn)

bulk MoS_2 has an indirect band gap of 1.29 eV[19]. Recently, monolayer and multilayer MoS_2 have been shown to have a carrier mobilities of up to 200 cm^2/Vs and 100 cm^2/Vs at room temperature, respectively, and a current on/off ratio of 1×10^8, which makes MoS_2 a promising candidate for incorporation into a new generation of more efficient transistors[20]. Moreover, monolayer MoS_2 has strong spin orbit coupling with a large spin splitting of up to 456 meV in the valence band originating from the d orbitals of the heavy metal atoms[21], due to the symmetry breaking[21,22]. Valley polarization in monolayer MoS_2 can be achieved with circularly polarized light[23,24]. Consequently, MoS_2 is also a fascinating material for spintronics applications based on spin and valley control[25,26]. MoS_2 also has potential in photoluminescence sensors[27], solar energy funnels[28], integrated circuit devices[29], chemical sensor[30], and photodiodes[31]. Recently, the magnetic and electronic properties of Fe_3O_4, MoS_2 and ferromagnetic metal/Mos_2 interfaces have been investigated[32–39] and the NiFe/MoS_2/NiFe Junction has been fabricated[40].

In this paper, we show based on the first principle calculations that Fe_3O_4 keeps a nearly fully spin polarized electron band at the interface between MoS_2 and Fe_3O_4 and no dead layer is formed at the interface. We also present the first report on the fabrication and characterization of MoS_2 based MTJs with ferromagnetic oxide electrode. The MTJ stacks in this work are Fe_3O_4-MoS_2-Fe_3O_4 trilayers grown on MgO (001) single crystal substrate. The quality of the MoS_2 barrier layer was investigated by X-ray photoemission spectroscopy (XPS), Raman spectroscopy, atomic force microscopy (AFM), and transmission electron microscopy (TEM). The magneto-transport properties were studied by the means of a physical property measurement system (PPMS, Quantum Design). A clear tunneling magnetoresistance (TMR) signal was observed at 200 K. Our results may be also valuable for understanding how MoS_2 can be used for other spintronic devices and applications.

Results

Electronic structure of Fe_3O_4/MoS_2/Fe_3O_4 junctions. We employed the projected augmented plane wave method (PAW)[41], implemented within the Vienna Ab Initio Simulation Package (VASP)[42]. The generalized gradient approximation[43] is used for the exchange-correlation energy. In our calculations, we use a rotated MoS_2 supercell constructed in a rectangular geometry and consider two reduced Fe_3O_4 unit cells containing 28 atoms each, separated by a 3 MoS_2 layers, as shown in Fig. 1e. We consider MoS_2 to be epitaxially grown on Fe_3O_4 as our experiment, thus the MoS_2 is strained to match the lattice of Fe_3O_4. All geometries are relaxed until the forces on the atoms are less than 0.02 eV/Å. Periodic boundary conditions are employed in the plane perpendicular to the transport direction (z direction), with a monkhorst-pack $6 \times 6 \times 1$ k-point grid for geometry optimization. In Fig. 1, we plotted the density of states (DOS) of B-site Fe (dark green ball) and Mo (dark blue ball) atoms far from the interface, and B-site Fe (light green ball) and Mo (light blue ball) atoms at the interface, for magnetization of the two Fe_3O_4 layers in parallel and anti-parallel configurations The MoS_2 at the interface becomes metallic behavior due to hybridization between Fe and S, which is consistent with the reports by another research group[40,44]. Significantly, despite the hybridization between the Fe and S, the interface Fe still keeps a nearly fully spin polarized electron band at the Fermi level, indicating that Fe_3O_4 keeps its half-metallic nature in Fe_3O_4/MoS_2/Fe_3O_4 junctions and no dead layer is formed at the interface. If we do not take into account the spin flip process when the spin polarized current tunneling through MoS_2, the TMR of a MTJ can be defined as: $TMR = \frac{2P_1P_2}{1 - P_1P_2}$, where P_1 and P_2 are the spin polarization of the two ferromagnetic electrodes. Thus, a significant high TMR is expected in Fe_3O_4/MoS_2/Fe_3O_4 junctions. In the following sections, we will describe the attempt to fabricate the Fe_3O_4/MoS_2/Fe_3O_4 MTJs.

Device preparation and characterization. The Fe_3O_4/MoS_2/Fe_3O_4 trilayer structures were grown on MgO (001) single crystal substrates. The thicknesses for the bottom and top Fe_3O_4 layers were 60 nm and 10 nm respectively. The Fe_3O_4 layers were prepared in a molecular beam epitaxy system (MBE) with a base pressure of 5×10^{-10} Torr. Reflection high energy electron diffraction (RHEED) was employed to confirm the epitaxial growth and establish the growth mode. Figure S1 shows RHEED patterns recorded in the [100] azimuth during growth, which indicates the pseudomorphic growth of the Fe_3O_4. Figure 2a shows the resistivity as a function of the temperature (R-T) for the bottom Fe_3O_4 layers. The Verwey transition is clearly present at 115 K which is close to well established bulk values, indicating the good quality of the bottom Fe_3O_4 layer. Details of the growth procedure and characterization are given elsewhere[45]. MoS_2 can be obtained by the top-down exfoliation methods[46], or by bottom up methods, such as transition metal sulfurization[47], molybdenum oxide sulfurization[48], decomposition of thiomolybdates[49], and van der Waals epitaxy[50]. To fabricate few- or single-layer MoS_2 devices, most studies use mechanical exfoliation or intercalation-assisted exfoliation of bulk MoS_2, which results in microscale flakes of random shapes and thicknesses. In this work, to achieve large-scale continuous MoS_2 films on the bottom Fe_3O_4 electrode, a thin Mo film was first deposited on the bottom Fe_3O_4 using an e-beam heated Mo source in the MBE system. After growth, the thin Mo layer was annealed at 500 °C with an oxygen partial pressure of 1×10^{-5} Torr for 30 minutes. Figure S1c shows the RHEED patterns of sample after annealing in oxygen indicating the epitaxial growth of MoO on the Fe_3O_4 layer which also guarantees a flat interface between MoS_2 and Fe_3O_4. To form MoS_2, the sample was removed from the MBE chamber and sulfurized at 700 °C for 1 min to 2 min in a furnace based on the well-established vapor phase growth technique[51]. The chemical composition of the MoS_2 layer was investigated by XPS (Fig. 2b). The Mo $3d_{5/2}$,

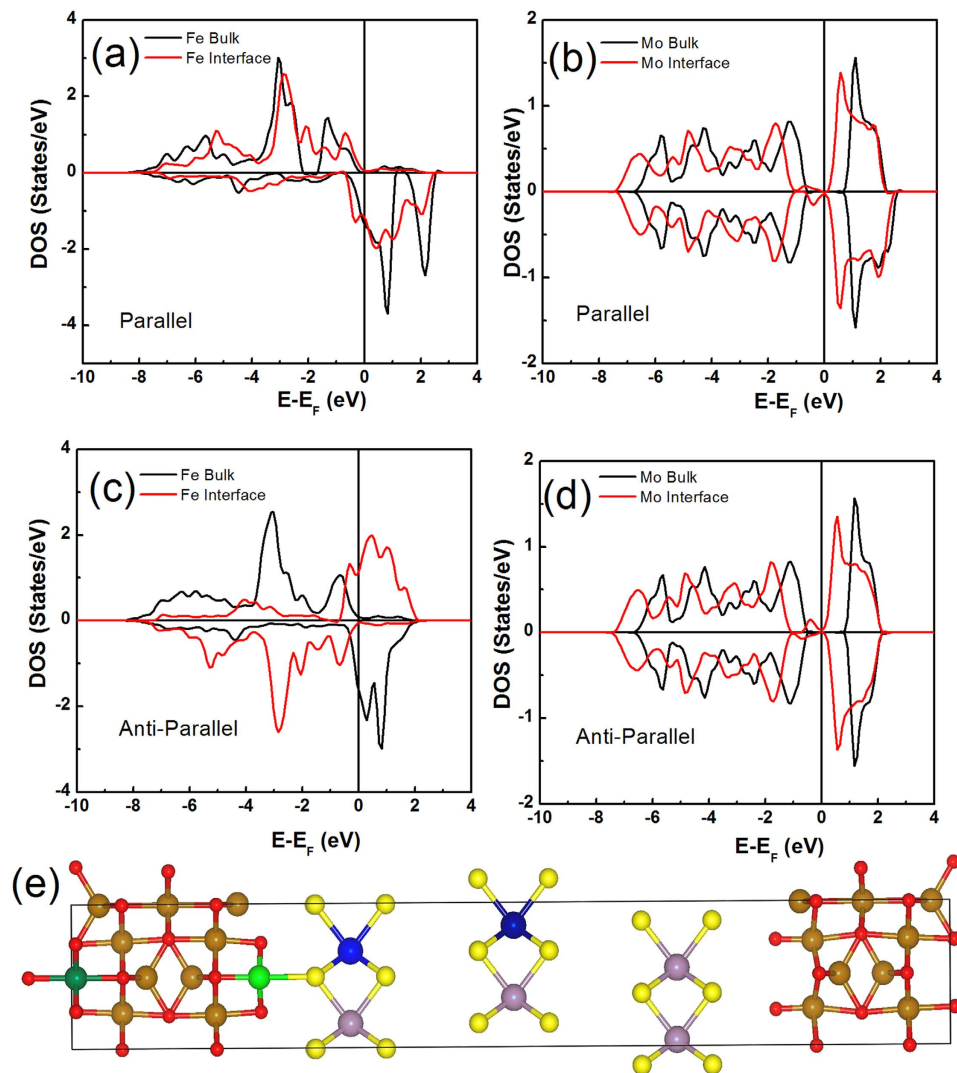

Figure 1. Electronic structure of $Fe_3O_4/MoS_2/Fe_3O_4$ junctions. Projected density of states of Fe (dark green ball) and Mo (dark blue ball) atoms far from the interface and Fe (light green ball) and Mo (light blue ball) atoms at the interface, for magnetization of the two Fe_3O_4 layers in parallel (**a,b**) or in anti-parallel configurations (**c,d**). (**e**) Atomic structure of the model used for density of states calculation.

Mo $3d_{3/2}$, and S 2s peaks have been consistently energy shifted in order to position the peak in the C 1s region at a binding energy (BE) of 284.7 eV. The peak positions for the Mo $3d_{5/2}$, Mo $3d_{3/2}$, and S 2s are 229 eV, 232 eV, and 226 eV respectively, which are consistent with the values for bulk MoS_2. From Fig. 2b, we can also estimate that the atomic ratio of Mo: S is approximately 1:2. Raman spectroscopy was used to further evaluate the quality of the MoS_2 layer. Figure 2c shows a Raman spectrum of the MoS_2 film collected by a Renishaw spectrometer with a 488 nm laser at room temperature. Strong signals for both the characteristic in-plane degenerate $E^1{}_{2g}$ and out-of plane A_{1g} modes are present at 406 cm^{-1} and 383 cm^{-1}, respectively. The peak positions are close to the positions expected for bulk MoS_2. The XPS and Raman results indicate the good quality of the MoS_2 layer.

The morphology of the MoS_2 was examined with AFM. The AFM image shown in Figure S2 indicates a uniform MoS_2 film on the Fe_3O_4. Additionally, the RMS roughness of this thin film is of 0.117 nm. The quality of the MoS_2/ Fe_3O_4 interface and thickness of MoS_2 layer were characterized by TEM. Figure 2d shows a typical TEM image of the MoS_2/ Fe_3O_4 bilayer on a MgO substrate. One can see from Fig. 2d that a 2 nm thick MoS_2 film is on top of the Fe_3O_4 layer with a sharp interface between the MoS_2 and Fe_3O_4 layers. Finally, the top Fe_3O_4 electrode was deposited. Two different size junctions ($10 \times 10\,\mu m^2$ and $400 \times 200\,nm^2$) were fabricated through several steps E-beam lithography and lift-off processes as described in the experimental section.

Magnetic and Transport properties. Figure 3a shows a schematic drawing of the $Fe_3O_4/MoS_2/Fe_3O_4$ junctions. When a bias current is applied perpendicular to the films, a spin-polarized current is injected

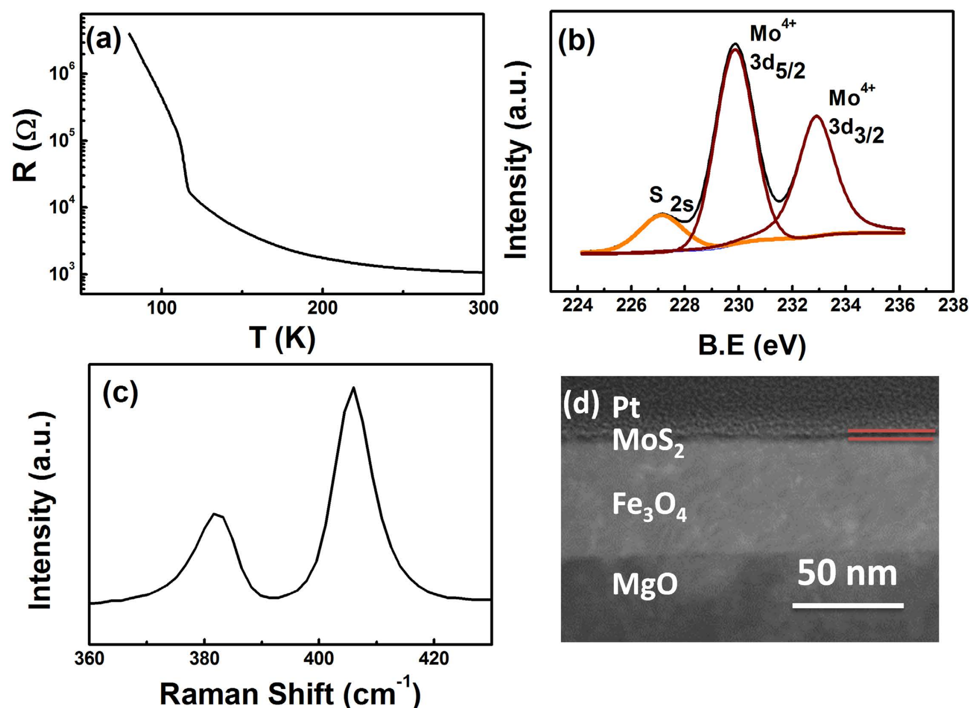

Figure 2. Raman and TEM characterization of Fe_3O_4/MoS_2/Fe_3O_4 trilayer structure. (**a**) R-T curve of the bottom Fe_3O_4 electrode, (**b**) X-ray photoemission spectroscopy compositional analysis of the MoS_2 layer, (**c**) Raman spectra of the MoS_2 barrier layer, (**d**) TEM characterization of MoS_2/Fe_3O_4 bilayer on a MgO substrate.

into the MoS_2 barrier layer from the top Fe_3O_4 electrode, which can then be detected by the bottom Fe_3O_4 electrode. It is known that the different thicknesses of the Fe_3O_4 layers will result in different coercivity fields[13]. Figure S3 shows the M (H) loops for 60 nm and 10 nm of Fe_3O_4 on MgO substrates. The coercivity fields for 60 nm of Fe_3O_4 and 10 nm of Fe_3O_4 at room temperature are 125 Oe and 60 Oe respectively. By applying an in-plane magnetic field, the magnetization states of the device can be tuned from a parallel (P) to an antiparallel (AP) configuration, or vice versa. Figure 3b–f show MR curves of Fe_3O_4/MoS_2/Fe_3O_4 junctions measured at different temperatures. The external magnetic field was applied in the film plane along the [100] direction. At 300 K, the resistance shows a linear response to the external field. While at low temperature, non-linear MR curves are observed. The linear MR behavior observed at room temperature is mainly due to spin-dependent transport across the anti-ferromagnetic (AF) anti-phase boundaries (APBs) in Fe_3O_4 layers[52,53]. To understand better the MR curves measured at low temperature, we show in Figure S4 the MR plots of the Fe_3O_4/MoS_2/Fe_3O_4 junctions measured with a field of up to 1 T. One can clearly see from Figure S4 that there are two main contributions to the MR: non-linear MR at low fields and linear MR at high fields due to spin-dependent transport across the AF APBs.

To demonstrate that the non-linear MR observed at low fields is not due to MR effects of the bottom or top Fe_3O_4 electrodes, we show in Fig. 4a MR curves for the bottom 60 nm thick Fe_3O_4 layer measured for different temperatures. Linear non-saturated MR curves are observed for temperatures above the Verwey temperature. Moreover, the MR ratio is significantly higher than that of the Fe_3O_4/MoS_2/Fe_3O_4 junctions. Below the Verwey temperature, the non-linear MR at low field is due to discrete changes in the entropy and the phonon-magnon interaction[52]. We also measured the MR of Fe_3O_4/MoS_2/Fe_3O_4 junctions without MoS_2 barrier (Figure S5). The MR curves are very similar to that for single Fe_3O_4 layer. Therefore, the non-linear MR observed in the Fe_3O_4/MoS_2/Fe_3O_4 junctions at low fields cannot be attributed to the MR effect of the bottom or top Fe_3O_4 electrodes. Figure 4b shows the R-T plot of the Fe_3O_4/MoS_2/Fe_3O_4 junctions.The resistance of the MTJ is one order of magnitude higher than that of solely the bottom Fe_3O_4 electrode and the R-T measurement shows no clear trace of the Verwey transition indicating that the resistance of the MTJ is dominated by the properties of the MoS_2 layer. We fitted the R-T curve with the relationship $R(T) \approx R_0 \exp(\frac{E_a}{K_B T})$, which gives an activation energy (E_a) of 72 meV. The obtained activation energy is about twice the value of that for the 60 nm Fe_3O_4 on MgO substrate and even larger than the activation energy for a single AF APB[52]. Note, while the Verwey transition is not observed in the R-T measurement, the temperature dependent magnetization (M-T) measurements still show a clear Verwey transition (Figure S6). To verify the observed non-linear MR at low fields is due to the TMR effect of the device, we show in Fig. 4c the current vs voltage (I-V) curve of the device measured

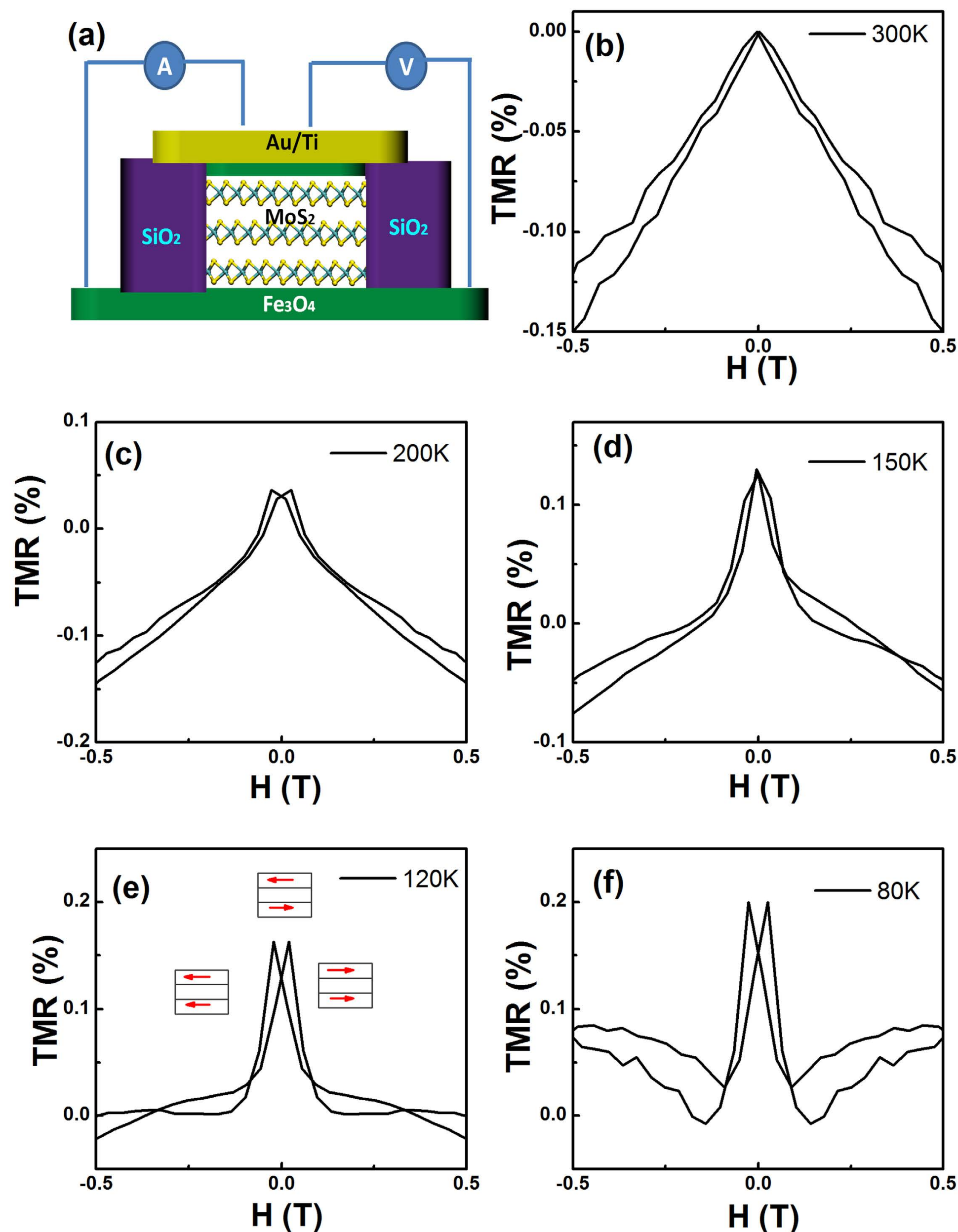

Figure 3. TMR of Fe_3O_4/MoS_2/Fe_3O_4 junctions. (**a**) Schematic drawing of the Fe_3O_4/MoS_2/Fe_3O_4 junctions. TMR curves for Fe_3O_4/MoS_2/Fe_3O_4 junctions measured at (**b**) 300 K, (**c**) 200 K, (**d**) 150 K, (**e**) 120 K, and (**f**) 80 K respectively.

at 300 K. Non-linear IV is observed. To confirm further this non-linear behavior, we show in Fig. 3d the dI/dV as a function of the bias voltage V. The quasiparabolic dependence between dI/dV and V also suggests that the non-linear MR observed at low fields is due to the TMR effect of the Fe_3O_4/MoS_2/Fe_3O_4 junctions. We can define the TMR ratio for the low field region as $TMR = \frac{R_{AP} - R_P}{R_P}$, where R_{AP} and R_P are resistances when the magnetization states of the device are in anti-parallel and parallel configurations respectively. Figure S7 shows the M (H) loop and MR curve for Fe_3O_4/MoS_2/Fe_3O_4 junction measured at 200 K. To clearly see the magnetization reversal process, we have drawn schematically the magnetization states of the device in Figure S7. Therefore, the non-linear MR observed at low fields is due to the magnetization alignments of two FM electrodes. Figure S8 summarizes the TMR ratio as a function of temperature. The TMR ratio increases with decreasing temperature and a TMR ratio of 0.2% is obtained at 80 K. We did not observe a sharp increase of the TMR ratio around Verwey transition which gives another indication that the non-linear MR at low fields is due to spin-dependent tunneling through the MoS_2 barrier layer. Although we did not obtain a TMR ratio as significant as that predicated by our calculation, our first attempt does suggest that MoS_2 can be used as a barrier material for Fe_3O_4 based

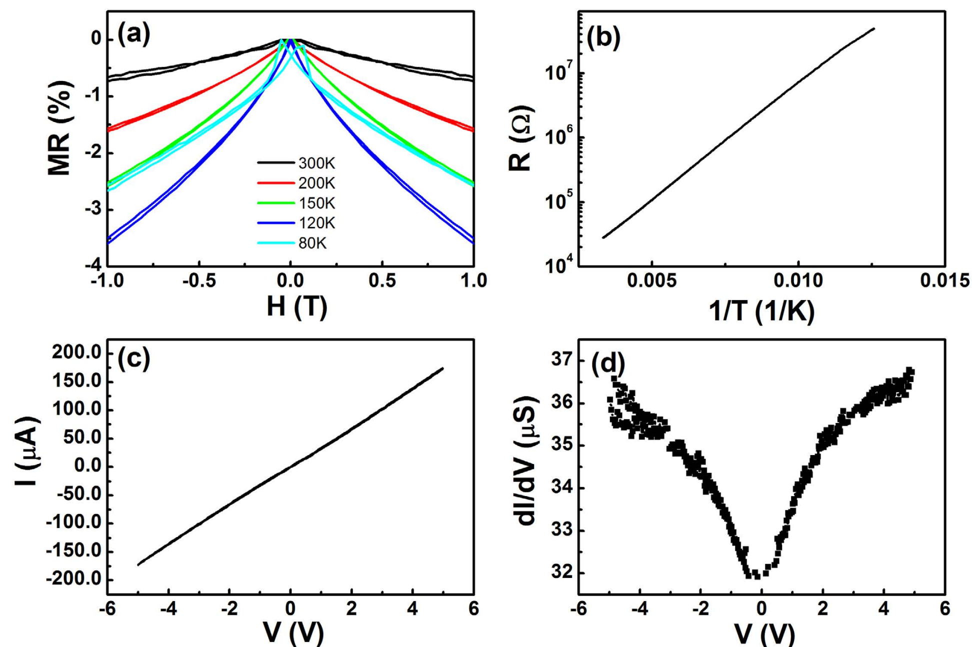

Figure 4. IV curve demonstrating the TMR effect of the device. (**a**) Temperature dependent MR curves for the bottom 60 nm thick Fe_3O_4 layer. (**b**) R-T for $Fe_3O_4/MoS_2/Fe_3O_4$ junctions measured at a bias of 0.5 V. (**c**,**d**) are IV and dI/dV curves for $Fe_3O_4/MoS_2/Fe_3O_4$ junctions measured at 300 K.

MTJ. One of the possible reasons for the reduced TMR ratio is that the quality of the interface between the MoS_2 and the top Fe_3O_4 may be not as good as the interface between the MoS_2 and the bottom Fe_3O_4 since the sample was removed from vacuum to produce the MoS_2 layer. To confirm this, Figure S9 shows the TMR ratio as a function of bias voltage measured at 200 K. One can see that TMR is asymmetric with respect to the bias voltage and has a maximum at a bias of −1 V. This asymmetry suggests that the quality of the two interfaces is different. The bottom Fe_3O_4/MoS_2 interface is atomically sharp, while the top Fe_3O_4/MoS_2 interface is rougher. It also indicates that the non-linear MR observed at low fields is due to the TMR effect of the $Fe_3O_4/MoS_2/Fe_3O_4$ junctions. Another possibility is that the bottom Fe_3O_4 may also be partially sulfurized during the sulfurization.

In conclusion, we show based on the first principle calculations and TMR characterization of $Fe_3O_4/MoS_2/Fe_3O_4$ junctions that MoS_2 can be a good barrier material for Fe_3O_4 based MTJs. Our calculations also indicate that junctions incorporating monolayer or bilayer MoS_2 are metallic. Our experimental results may pave the way for the application of MoS_2 in spintronics.

Methods

Growth of Fe_3O_4-MoS_2-Fe_3O_4 trilayers. The Fe_3O_4-MoS_2-Fe_3O_4 trilayers were grown on MgO (001) single crystal substrates using a MBE system (DCA MBE M600, Finland) with a base pressure of 5×10^{-10} Torr. The substrates were chemically cleaned prior to their insertion into the growth chamber and then cleaned *in situ* at 600 °C in UHV for 1 hour. The growth conditions for Fe_3O_4 can be found elsewhere. The thicknesses for the bottom and top Fe_3O_4 layers are 60 nm and 10 nm respectively. To grow MoS_2, a thin Mo film were first deposited by e-beam from a Mo source. Subsequently, the thin Mo layer was annealed at 500 °C with an oxygen partial pressure of 1×10^{-5} Torr for 30 mins. Then the sample was taken out and sulfurized at 700 °C for 1 min to 2 min in a chemical vapor deposition (CVD) furnace to form MoS_2 based on the vapor phase growth technique. This short sulfurization time prevents a deeper sulfurization of the Fe_3O_4 layer in agreement with the XPS analysis.

Device fabrication. A multistep process was used to fabricate the Fe_3O_4-MoS_2-Fe_3O_4 junctions with two different sizes ($10 \times 10\,\mu m^2$ and $400 \times 200\,nm^2$). The resistance-area (RA) of the junction is around $10^7\,\Omega\,\mu m^2$ at room temperature and remains constant irrespective to the junction size. A Negative tone S1820 and MA N2403 were used for UV lithography and e-beam lithography respectively, followed by ion milling and the post exposure lift-off was carried out after SiO_x deposition to insulate the top and bottom contacts. A top contact of Ti 6 nm/Au 50 nm was deposited by evaporation with subsequent lift off.

Characterization of the Fe_3O_4-MoS_2-Fe_3O_4 junctions. The magneto-transport behavior of the Fe_3O_4-MoS_2-Fe_3O_4 junctions was examined by means of a physical property measurement system

(PPMS, Quantum Design). X-ray photoelectron spectrometer (XPS) measurements were performed in an Omicron Nanotechnology Spectroscopy system equipped with an Ar ion miller in the preparation chamber. Raman spectra was collected using a Renishaw InVia spectrometer with a 488 nm laser at room temperature.

References

1. Walz, F. The verwey transition—a topical review. *J. Phys. Condens. Matter* **14,** R285 (2002).
2. Ziese, M. Extrinsic magnetotransport phenomena in ferromagnetic oxides. *Rep. Prog. Phys.* **65,** 143 (2002).
3. Brabers, J. H. V. J., Walz, F. & Kronuller, H. The influence of a finite bandwidth on the Verwey transition in magnetite. *J. Phys. Condens. Matter.* **12,** 5437 (2002).
4. Ramos, R. *et al.* Observation of the spin Seebeck effect in epitaxial Fe_3O_4 thin films. *Appl. Phys. Lett.* **102,** 072413 (2013).
5. Liao, Z. M. *et al.* Spin-filter effect in magnetite nanowire. *Nano Lett.* **6,** 1087 (2006).
6. Gooth, J. *et al.* Gate voltage induced phase transition in magnetite nanowires. *Appl. Phys. Lett.* **102,** 073112 (2013).
7. Lee, S. *et al.* Electrically driven phase transition in magnetite nanostructures. *Nature Mater.* **7,** 130 (2008).
8. Wong, J. J. I., Swartz, A. G., Zheng, R. J., Han, W. & Kawakami, R. K. Electric field control of the verwey transition and induced magnetoelectric effect in magnetite. *Phys. Rev. B* **86,** 060409 (2012).
9. Fernández-Pacheco, A. *et al.* Giant planar hall effect in epitaxial Fe_3O_4 thin films and its temperature dependence. *Phys. Rev. B* **78,** 212402 (2008).
10. Wu, H. C. *et al.* Transversal magneto-resistance in epitaxial Fe_3O_4 and Fe_3O_4/NiO exchange biased system. *Appl. Phys. Lett.* **101,** 052402 (2012).
11. Wu, H. C., Mryasov, O. N., Abid, M., Radican, K. & Shvets, I. V. Magnetization states of all-oxide spin valves controlled by charge-orbital ordering of coupled ferromagnets. *Sci. Rep.* **3,** 1830 (2013).
12. Li, X., Gupta, A., Xiao, G., Qian, W. & Dravid, V. Fabrication and properties of heteroepitaxial magnetite tunnel junctions. *Appl. Phys. Lett.* **73,** 3282 (1998).
13. Wu, H. C., Arora, S. K., Mryasov, O. N. & Shvets, I. V. Antiferromagnetic interlayer exchange coupling between Fe_3O_4 layers across a nonmagnetic MgO dielectric layer. *Appl. Phys. Lett.* **92,** 182502 (2008).
14. Novoselov, K. S. *et al.* Two-dimensional gas of massless dirac fermions in graphene. *Nature* **438,** 197 (2005).
15. Zhang, Y., Tan, Y. W., Stormer, H. L. & Kim, P. Experimental observation of the quantum Hall effect and Berry's phase in graphene. *Nature* **438,** 201 (2005).
16. Liao, Z. M. *et al.* Magnetoresistance of Fe_3O_4-graphene-Fe_3O_4 junctions. *Appl. Phys. Lett.* **98,** 052511 (2011).
17. Han, W. *et al.* Tunneling spin injection into single layer graphene. *Phys. Rev. Lett.* **105,** 167202 (2010).
18. Mak, K. F., Lee, C., Hone, J., Shan, J. & Heinz, T. F. Atomically Thin MoS_2: a new direct-gap semiconductor. *Phys. Rev. Lett*. **105,** 136805 (2010).
19. Kam, K. K. & Parkinson, B. A. Detailed photocurrent spectroscopy of the semiconducting group VIB transition metal dichalcogenides. *J. Phys. Chem*. **86,** 463 (1982).
20. Radisavljevic, B., Radenovic, A., Brivio, J., Giacometti, V. & Kis, A. Single-layer MoS_2 transistors. *Nature Nanotech*. **6,** 147 (2011).
21. Zhu, Z. Y., Cheng, Y. C. & Schwingenschlögl, U. Giant spin-orbit-induced spin splitting in two-dimensional transition-metal dichalcogenide semiconductors. *Phys. Rev. B* **84,** 153402 (2011).
22. Ellis, J. K., Lucero, M. J. & Scuseria, G. E. The indirect to direct band gap transition in multilayered MoS2 as predicted by screened hybrid density functional theory. *Appl. Phys. Lett*. **99,** 261908 (2011).
23. Yao, W., Xiao, D. & Niu, Q. Valley-dependent optoelectronics from inversion symmetry breaking. *Phys. Rev. B* **77,** 235406 (2008).
24. Xiao, D., Liu, G. B., Feng, W., Xu, X. & Yao, W. Coupled spin and valley physics in monolayers of MoS_2 and other group-VI dichalcogenides. *Phys. Rev. Lett.* **108,** 196802 (2012).
25. Zeng, H., Dai, J., Yao, W., Xiao, D. & Cui, X. Valley polarization in MoS_2 monolayers by optical pumping. *Nat. Nanotech.* **7,** 490 (2012).
26. Mak, K. F., He, K., Shan, J. & Heinz, T. F. Control of valley polarization in monolayer MoS_2 by optical helicity. *Nat. Nanotech.* **7,** 494 (2012).
27. Yin, Z. Y. *et al.* Single-layer MoS_2 phototransistors. *ACS Nano* **6,** 74 (2012).
28. Feng, J., Qian, X., Huang, C.-W. & Li, J. Strain-engineered artificial atom as a broad-spectrum solar energy funnel. *Nat. Photon.* **6,** 866 (2012).
29. High, A. A., Novitskaya, E. E., Butov, L. V., Hanson, M. & Gossard, A. C. Control of exciton fluxes in an excitonic integrated circuit. *Science* **321,** 229 (2008).
30. Lee, K., Gatensby, R., McEvoy, N., Hallam, T. & Duesberg, G. S. High-performance sensors based on molybdenum disulfide thin films. *Adv. Mater.* **25,** 6699 (2013).
31. Yim, C. *et al.* Heterojunction hybrid devices from vapor phase grown MoS_2. *Sci. Rep.* **4,** 5458 (2014).
32. Mi, W. B., Shen, J. J., Jiang, E. Y. & Bai, H. L. Microstructure, magnetic and magneto-transport properties of polycrystalline Fe_3O_4 films. *Acta Mater.* **55,** 1919 (2007).
33. Senn, M. S., Wright, J. P. & Attfield, J. P. Charge order and three-site distortions in the verwey structure of magnetite. *Nature* **481,** 173 (2012).
34. Mi, W. B., Guo, Z. B., Wang, Q. X., Yang, Y. & Bai, H. L. Charge ordering in reactive sputtered (100) and (111) oriented epitaxial Fe_3O_4 films. *Scripta Mater.* **68,** 972 (2013).
35. Feng, N. *et al.* Magnetism by interfacial hybridization and p-type doping of MoS_2 in Fe_4N/MoS_2 superlattices: a first-principles study. *ACS Appl. Mater. Interf.* **6,** 4587 (2014).
36. Yin, M. Y., Wang, X. C., Mi, W. B. & Yang, B. H. First principles prediction on the interfaces of Fe/MoS_2, Co/MoS_2 and Fe_3O_4/MoS_2. *Comput. Mater. Sci.* **99,** 326 (2015).
37. Zhang, X. J., Mi, W. B., Wang, X. C., Cheng, Y. C. & Schwingenschlögl, U. The interface between Gd and Monolayer MoS_2: a first-principles study. *Sci. Rep*. **4,** 7368 (2014).
38. Zhang, X. J., Mi, W. B., Wang, X. C., Cheng, Y. C. & Schwingenschlögl, U. First principles prediction of the magnetic properties of Fe-X_6 (X=S, C, N, O, F) doped monolayer MoS_2. *Sci. Rep.* **4,** 3987 (2014).
39. Cheng, Y. C., Zhu, Z. Y., Mi, W. B., Guo, Z. B. & Schwingenschlögl, U. Prediction of two-dimensional diluted magnetic semiconductors: Doped monolayer MoS_2 systems. *Phys. Rev. B* **87,** 100401(R) (2013).
40. Wang, W. *et al.* Spin-Valve Effect in NiFe/MoS_2/NiFe Junctions. *Nano Lett*. (2015), doi: 10.1021/acs.nanolett.5b01553.
41. Kresse, G. & Hafner, J. Ab initio molecular dynamics for liquid metals. *Phys. Rev. B* **47,** R558 (1993).
42. Payne, M. C., Teter, M. P., Allan, D. C., Arias, T. A. & Joannopoulos, J. D. Iterative minimization techniques for ab initio total-energy calculations: molecular dynamics and conjugate gradients. *Rev. Mod. Phys.* **64,** 1045 (1992).
43. Perdew, J. P., Burke, K. & Ernzerhof, M. Generalized gradient approximation made simple. *Phys. Rev. Lett.* **77,** 3865 (1996).

44. Dolui, K., Narayan, A., Rungger, I. & Sanvito, S. Efficient spin injection and giant magnetoresistance in Fe/MoS_2/Fe junctions. *Phys. Rev. B* **90,** 041401(R) (2014).
45. Arora, S. *et al.* Giant magnetic moment in epitaxial Fe_3O_4 thin film. *Phys. Rev. B* **77,** 134443 (2008).
46. Splendiani, A. *et al.* Emerging photoluminescence in monolayer MoS_2. *Nano Lett.* **10,** 1271 (2010).
47. Kim, D. *et al.* Toward the growth of an aligned single-layer MoS_2 film. *Langmuir* **27,** 11650 (2011).
48. Lee, Y. H. *et al.* Synthesis of large-area MoS_2 atomic layers with chemical vapor deposition. *Adv. Mater.* **24,** 2320 (2012).
49. Liu, K. K. *et al.* Growth of large-area and highly crystalline MoS_2. *Nano Lett.* **12,** 1538 (2012).
50. Ji, Q. *et al.* Epitaxial monolayer MoS_2 on mica with novel photoluminescence. *Nano Lett.* **13,** 3870 (2013).
51. Gatensby, R. *et al.* Controlled synthesis of transition metal dichalcogenide thin films for electronic applications. *Appl. Surf. Sci.* **297,** 139 (2014).
52. Wu, H. C. *et al.* Probing one antiferromagnetic anti-phase boundary and single magnetite domain using nanogap contacts. *Nano Lett.* **10,** 1132 (2010).
53. Eerenstein, W., Palstra, T. T. M., Saxena, S. S. & Hibma, T. Spin-polarized transport across sharp antiferromagnetic boundaries. *Phys. Rev. Lett.* **88,** 247204 (2002).

Acknowledgements

This work was supported by Beijing Institute of Technology Research Fund Program for Young Scholars, Science Foundation of Ireland (SFI) (Contract No. 06/IN.1/I91, 10/IN.1/I3030), National Plan for Science and technology (Nos. NPST 1598–02 and NPST 1466–02) of King Abdulaziz City for Science and Technology. H.C.W., MA.A., and MO.A. thank Saudi Aramco for the financial support (project No. 6600028398). O.M. and A.S. acknowledge the financial support by the Bolashak Program funded by the Kazakhstan government. We would like to thank Prof. O.N. Mryasov for reading the manuscript and giving valuable comments.

Author Contributions

H.C.W. conceived the study. O.M., A.S. and C.C. grew the sample. A.S., H.J.X., and M.O.H.A. fabricated the sample. H.C.W. performed the magnetic and transport measurements. A.K., A.M., and H.Z.Z. carried out the TEM measurements. R.G. and G.S.D. sulfurized the sample. J.J.W. and MOU.A. performed the Raman characterization. H.L., L.Y. and I.V.S. gave scientific advice. H.C.W. wrote the manuscript. All authors discussed the results and commented on the manuscript.

Additional Information

Supplementary information accompanies this paper at http://www.nature.com/srep

Competing financial interests: The authors declare no competing financial interests.

How to cite this article: Wu, H.-C. *et al.* Spin-dependent transport properties of Fe_3O_4/MoS_2/Fe_3O_4 junctions. *Sci. Rep.* **5**, 15984; doi: 10.1038/srep15984 (2015).

This work is licensed under a Creative Commons Attribution 4.0 International License. The images or other third party material in this article are included in the article's Creative Commons license, unless indicated otherwise in the credit line; if the material is not included under the Creative Commons license, users will need to obtain permission from the license holder to reproduce the material. To view a copy of this license, visit http://creativecommons.org/licenses/by/4.0/